


The comparative anti-obesity potential of *Lagerstroemia speciosa* (L.) leaf extracts and their synthesized gold nanoparticles by downregulation of PPAR- γ , C/EBP- α , and FABP4/aP2 gene expression

Tarsem Nain¹, Mahendra Bishnoi², Navpreet Kaur², Santosh Kumar Tiwari¹, Jaya Parkash Yadav^{1*} 

¹Department of Genetics, Maharshi Dayanand University, Rohtak, Haryana, India.

²Department of Nutritional Science, National Agri-Food Biotechnology Institute, Mohali, Punjab, India.

ARTICLE INFO

Article history:

Received on: 14/05/2025

Accepted on: 12/08/2025

Available online: 25/11/2025

Key words:

Lagerstroemia speciosa,
Lipid content,
Reactive oxygen species,
Triglyceride level,
C/EBP- α ,
PPAR- γ , and ap2 gene expression.

ABSTRACT

The rising worldwide obesity rate is associated with various metabolic disorders such as hypertension, stroke, type 2 diabetes, cancer, and exacerbation of health challenges throughout the world. *Lagerstroemia speciosa* offers multiple health benefits, including anticancer, cardiovascular, nephroprotective, hypertension, insulin sensitivity, anti-diabetic, and inflammation-related conditions. The present study explored the comparative anti-adipogenic effects of different extracts and spherical gold nanoparticles (Au-NPs) synthesized with fresh *L. speciosa* leaf (LS-Au-NPs) using 3T3-L1 mature adipocytes. Cell viability was assessed using an MTT assay, and reactive oxygen species (ROS) production was evaluated using the 2',7'-dichlorodihydrofluorescein diacetate method. The gene expression pattern of key adipogenic genes, peroxisome proliferator-activated receptor gamma, CCAAT/enhancer binding protein alpha, and ap2 was quantified using reverse transcription polymerase chain reaction. Results demonstrated that leaf extracts and Au-NPs were non-toxic to 3T3-L1 cells up to a specific concentration and significantly reduced ROS generation, lipid accumulation, and triglyceride content in induced obese cells. Aqueous, supercritical fluid extraction (SFE) extract, and AuNPs exhibited the most potent effects, while the methanol extract showed moderate effects, and the n-hexane extract had negligible effects on gene expression regulation. Altogether, these results showed that all effective treatments significantly downregulated the transcriptional adipogenic genes, reflecting their potent anti-obesity potential. SFE exhibited more pronounced effects due to the non-toxicity of the solvent. Thus, the plant leaf is a rich source of phenolic and flavonoid compounds that coat the surface of Au-NPs and help to reduce excess lipid and triglyceride content in the cells.

1. INTRODUCTION

Obesity is a significant health concern throughout the world, impacting billions of people. The current trends indicate that by 2030, approximately 3.3 billion individuals and 57.8% of adults worldwide will experience overweight and obesity [1]. It is a metabolic syndrome that develops when the energy consumption rate exceeds the energy utilization rate, leading to an increase in fat cell number and size through hypertrophy and hyperplasia [2]. Abnormal expansion can contribute to various endocrine and metabolic illnesses, including hypertension, insulin resistance, and dyslipidemia, all of which elevate the risk of type 2 diabetes mellitus disease [3]. Major drivers of this epidemic

include diet with high in cholesterol, sugars, and saturated fat, combined with a sedentary lifestyle that can lead to disruption of gene expression and transcription factor activity, promoting triglyceride content and lipid accumulation within body organs [4]. Furthermore, an extremely high-fat diet leads to hyperlipidemic conditions, which subsequently increase the production of reactive oxygen species (ROS), differentiation of adipocytes, and the fatty acid oxidation process [5]. Peroxisome proliferator-activated receptor gamma (PPAR- γ), CCAAT/enhancer binding protein alpha (C/EBP- α), and ap2 are the most critical transcription factor that controls the process of lipid storage, adipocyte differentiation, and fatty acid oxidation process [6]. The whole process of adipogenesis occurs in two stages: Clonal expansion and terminal differentiation. During expansion, cells express specific proteins and activate transcription factors C/EBP- α and PPAR- γ . These activated transcription factors then perform the function of terminal differentiation and accumulation of lipid droplets [7].

*Corresponding Author:

Jaya Parkash Yadav,

Department of Genetics,

Maharshi Dayanand University, Rohtak-124001, Haryana, India.

E-mail: yadav1964@rediffmail.com

Approved standard drugs (orlistat and sibutramine) primarily emphasize energy intake reduction, while, till now, no approved medication can target the energy expenditure process [8]. Despite that, persistent use of anti-obesity synthetic drugs can lead to severe effects on the whole body's organs [9]. Therefore, the development of novel, natural, traditional treatments that effectively cure obesity and related metabolic disorders with severe effects is essential. Recent research has shown that various medicinal herbs offer tremendous beneficial effects in addressing obesity complications [10]. Their natural compounds promote lipolysis, inhibit adipogenesis, and restrict lipid droplet formation within 3T3-L1 preadipocytes by downregulating PPAR- γ , C/EBP- α , and ap2 genes.

Lagerstroemia speciosa is a beneficial medicinal plant from the Lythraceae family, native to tropical regions of Australia, Malaysia, the Philippines, India, and southern China [11]. More than 35 phytoconstituents, namely ellagic acid, corosolic acid, quercetin, and flavones, have been identified and isolated from the *L. speciosa* [12]. The plant performs diverse biological activities, namely hepatoprotective, nephroprotective, and inhibition of tumor necrosis factor alpha production [13], xanthine oxidase inhibition [14], antimicrobial, antioxidant, anticancer, anti-obesity, hypolipidemic [11], analgesic, gastrointestinal [15], diuretic, thrombolytic [16], cardiovascular [17], anti-diabetic, anti-cancer [18], anti-hepatic steatosis [19], anti-ulcerative colitis, treat hypertension [20], urinary dysfunctions, and gastrointestinal disturbances [21].

Previous investigations demonstrated that *L. speciosa* leaf extract shows promising *in vivo* and *in vitro* anti-cancer activity against the A549 cell line and lung tumorigenesis mouse model, respectively [22]. The presence of key phytochemicals such as corosolic acid and ethanolic extract shows tremendous anti-adipogenic/obesity activity in high-fat-diet-induced albino rats [23]. Treatment with DLBS3233 fraction mitigates insulin resistance in women with polycystic ovary syndrome [24]. Synthesized silver nanoparticles from the flower buds of *L. speciosa* against clinical pathogenesis and dose-dependent anti-cancer activity on osteosarcoma (MG-63) cells [25].

A practical approach to increasing the bioavailability of plant-based compounds is the development of nanosized formulations [26]. Nanoparticles improve the therapeutic efficacy and bioavailability of phytochemicals by increasing their surface area. Smaller nanoparticles are more easily taken up by macrophage cells, enhancing therapeutic rates [27]. Despite promising preclinical findings, clinical evidence supporting the therapeutic efficacy of plant molecular analysis in the context of anti-obesity remains limited. Therefore, the present study has been taken to evaluate the comparative effects of aqueous methanol, Supercritical Fluid Extraction (SFE), n-hexane, and synthesized gold nanoparticles (Au-NPs) on lipid accumulation, ROS generation, triglyceride levels, and regulation of relative adipogenic m-RNA gene expression in mature adipocytes. The novelty of the present work lies in the innovative nanoparticle formulation from *L. speciosa* and the comparative extraction approach, enabling enhanced anti-adipogenic activity over conventional extracts.

2. MATERIALS AND METHODS

2.1. Sample Collection

Based on the morphology and literature study, fresh mature leaf tissue samples in the early summer season were collected from the local area of M.D. University, Rohtak (Latitude 28.8770° N and Longitude

76.6211° E), having 28.8770° N and 76.6211° E geographical attributes. All samples are carefully brought to the laboratory for further processing. Plant samples are authenticated by the CSIR-National Institute of Science Communication and Policy Research (CSIR-NIScPR), Dr. K S Krishnan Marg, Pusa Campus, New Delhi - 110012, having authentication no. NIScPR/RHMD/Consult/2022/4075-76.

2.2. Extract Preparation using Different Solvents

Collected samples were rinsed with tap water and deionized water to remove extraneous matter. The leaf tissue samples were air-dried and chopped into fine pieces, followed by grinding into a fine powder using a mixer grinder, and then extracted with different solvents, such as aqueous, methanol, and n-hexane, by taking 10–15 g fresh tissue samples in 300 mL distilled water, boiling for 35 min. The extracts were filtered using the Whatman No. 1 filter paper, and the solvent was subsequently evaporated by keeping the samples in a rotary evaporator InKarp (model no RV21A & RV31A Rotary Evaporator) at 37°C [28].

2.3. Leaf Extract Preparation using SFE

Sample jackets of machine vials are packed with 10 g of leaf-powdered plant material. Static extraction mode was operated during extraction by using CO₂ as a carrier gas. The flow rates were kept at 1 mL/min at 240°C and 260 MPa pressure in the SFE extractor machine. The sample was collected in the collection tube, which was evaporated at 37°C, i.e., room temperature, to eliminate residual CO₂. The extract was then lyophilized (Hyper cool HC3110). The lyophilized samples were stored at 4°C for further analysis [29].

2.4. Phytochemical Screening

Preliminary phytochemical screening was performed for terpenoids, protein and amino acids, glycosides, alkaloids, saponins, carbohydrates, steroids, flavonoids, and phenols as previously described method with slight modifications [30].

2.5. Synthesis of Au-NPs

Au-NPs were synthesized from *L. speciosa* leaves using a standard protocol with slight modifications [31]. In a 500 mL conical flask, the fresh filtered leaf extract was reacted with a 0.5 mM concentration solution of tetrachloroaurate salt (HAuCl₄) in 9:1 (HAuCl₄ salt: plant extract) at room temperature under constant static conditions. The reaction mixture immediately changed color from slightly pale yellow to ruby pink in 3 min, confirming the synthesis of Au/*L. speciosa* nanoparticles. Ultraviolet (UV)-visible spectra were performed at 546 nm to confirm the Au-NPs synthesis.

2.6. Characterization of Synthesized Nanoparticles

Nanoparticle reduction was initially confirmed using a double-beam UV-vis spectrophotometer (Shimadzu, 2450). The reduced nanoparticle emulsion was dried into powder form using a Hyper-COOL HC3110 lyophilizer. Fine-dried crystal samples were collected in air-tight amber tubes for further structural and compositional analysis using field emission scanning electron microscopy (FE-SEM) at Guru Jambheshwar University, Hisar, Transmission Electron Microscopy (TEM) at SAIF-CIL Panjab University, Chandigarh, Fourier-Transform Infrared Spectroscopy (FTIR), and X-ray diffraction (XRD) at the Department of Physics at Maharshi Dayanand University, Rohtak. The functional group of compounds responsible for bio-reduction was analyzed using FTIR. The size and stability were studied using a Zeta-Sizer and Zeta Potential. The crystallinity

of nanoparticles was investigated by XRD. Shape and morphological characters were analyzed using SEM. The average size distribution was studied using TEM.

2.6.1. Zeta potential/zeta sizer study

The Malvern 7.13 particulate analyzer system was used to measure the stability potential of the nanomaterial. The ± 30 -mV zeta potential value of the dissolved suspension signifies strong electrostatic repulsion and stable dispersion of Au-NPs. The ± 20 mV potential is necessary for the steric and electrostatic combined effect [32].

2.6.2. Attenuated total reflection (ATR)-FTIR study

The sample (2 mg) was prepared by thoroughly distributing the Au-NPs in a matrix of dry KBr, which was compressed to form a transparent disc. KBr served as a reference for analyzing the test material. The spectra were scanned in the range of 600–3600 cm^{-1} at a resolution of 4 cm^{-1} using an ATR-FTIR instrument (Bruker) [33].

2.6.3. XRD analysis

The crystallinity of the synthesized nanoparticles was examined using a benchtop Rigaku MiniFlex 600 X-ray diffractometer equipped with Cu K α radiation ($\lambda = 1.540598 \text{ \AA}$) operated at 40 kV voltage and 15 mA current. The diffraction patterns of nanoparticles were traced in the diffraction range of 2θ , having $10\text{--}90^\circ$ [34]. The average crystallite size of the Au-NPs was calculated using the Debye-Scherrer equation, which is expressed as $D = \frac{K\lambda}{\alpha \cos \theta}$

2.6.4. SEM

The FE-SEM was employed to examine the surface morphology of the synthesized Au-NPs [35]. The samples were coated on a slide and then mounted with platinum in an auto fine coater. After that, the sample was subjected to examination using FE-SEM JEOL (Semtrac Japan).

2.6.5. TEM

An aliquot of 10 μL sample was placed on a copper grid covered with a formvar-carbon film of 300 mesh size. The covered copper grid was undisturbed for drying for at least 1 h and then placed in a vacuum chamber [36]. Interplanar spacing of crystal planes was analyzed at a voltage of 200 kV with high-resolution TEM (HR-TEM) micrograph digital analysis (version 3.0).

2.7. 3T3-L1 cell culture and maintenance

3T3-L1 fibroblasts were purchased from American Type Culture Collection (ATCC) and cultured in basal medium [Dulbecco's Modified Eagle Medium (DMEM, Cat. no. 12-604F, Lonza, Basel, Switzerland) supplemented with 1% penicillin-streptomycin (Cat. no. 15140122, GIBCO) and 10% v/v FBS (Cat. no. ATCC 092910154, MP Biomedicals). Cell cultures were maintained in accordance with ATCC procedures.

2.7.1. Differentiation of 3T3-L1 cells

80% confluent, 3T3-L1 pre-adipocytes were differentiated into adipocytes by supplementing the differentiation medium (basal media supplemented with 0.5 mM IBMX, 1 $\mu\text{g/ml}$ insulin, and 0.1 μM DMS) for 48h. Subsequently, the induced cells were cultured in a maintenance medium (basal medium supplemented with 1 $\mu\text{g/ml}$ insulin) for 8–14 days, with media replacement on alternate days.

2.8. Cell Viability Assessment

Percent cell viability was assessed using an MTT assay. 3T3-L1 preadipocyte cells were seeded at a density of 1×10^4 cells per well

into a 96-well plate and incubated overnight prior to achieving 80% confluency; the cells were treated with different concentrations, namely 50, 100, and 200 $\mu\text{g/ml}$ of leaf extract, and their synthesized Au-NPs for 24 h. Upon treatment, the media were changed with MTT (1 mg/mL), and cells were kept in the dark for 4 h at 37°C. Resulting formazan crystals produced by the metabolically active/functional cells were liquefied in DMSO, and the absorption value was recorded at 570 nm with the help of a microplate reader (Spectra Max M5e, Molecular Devices LLC), according to the previously described method [37]. The cytotoxicity values of the tested compounds and nanoparticles are determined using the formula:

$$\% \text{ Cell viability} = \frac{\text{OD of test sample (mean)}}{\text{OD of Control (mean)}} \times 100$$

2.9. Lipid Staining

Cells were thoroughly washed with phosphate-buffered saline (PBS) and fixed with 4% (v/v) formaldehyde in PBS for 20 min. Cells were rinsed thrice with PBS and 60% isopropanol for 5 min. Subsequently, staining was performed with 0.2% Oil-Red-O (ORO) solution (Cat. no O-0625, Sigma-Aldrich) prepared in isopropyl alcohol (IPA) for 10 min at room temperature. After staining, the cells were washed with 60% IPA to remove excess dye, and the stained lipids were examined at $\times 20$ magnification using a microscope. Stained cells were subjected to incubation in 100% isopropanol for 10 min to quantify lipid accumulation and extract the ORO dye from the lipid droplets. Absorbance was recorded at 570 nm using a microplate reader [38].

2.10. ROS Analysis

ROS production was assessed using 2',7'-dichlorodihydrofluorescein diacetate (H_2DCFDA) dye to measure ROS levels. 3T3-L1 preadipocytes were cultured to full confluence, induced to differentiate into adipocytes, and subjected to specified treatments. Following treatment (50, 100, and 200 $\mu\text{g/ml}$), the cells were rinsed with PBS and exposed to 10 μM $\text{H}_2\text{DCF-DA}$ dye for 30 min in a dark condition within an incubator maintained at 37°C with 5% CO_2 . Subsequently, the fluorochrome was removed, and the cells were rinsed with PBS before being examined under fluorescence microscopy, employing appropriate excitation and emission wavelengths for green fluorescence between 485 nm and 530 nm, respectively [39].

2.11. Triglycerides Estimation

The cells underwent an 8-day differentiation process followed by treatment with various doses of 50, 100, and 200 $\mu\text{g/ml}$. After treatment, the cells underwent two washes with PBS buffer, and then, 2 mL of hexane: IPA (3:2) solution was added and incubated for 30 min. The resulting supernatant was transferred to fresh, labeled tubes, and placed in a fume hood for evaporation. The lipids were then reconstituted in 0.4 mL of a standard diluent ($\times 1$). In a 96-well plate, samples and standards (10 μL each) were added to designated wells, followed by 150 μL of a diluted enzyme mixture solution. The plate was gently covered and kept in the dark for 30 min at 37°C. Absorbance was subsequently recorded at 530–550 nm using a microplate reader [40].

2.12. RNA Extraction and Gene Expression Analysis

The gene expression was performed according to standard reverse transcription polymerase chain reaction (PCR) MIQE guidelines [41]. Total RNA was extracted from adipocytes after 48 h of treatment from days 8 to 10 using a previously standardized triazole (RNA extraction

agent) based method [42]. The cells were washed in PBS and homogenized in 1 mL of triazole. The homogenate was then vortexed, and 200 μ L ice-cold chloroform was added, followed by incubation for 3–5 min. The mixture was centrifuged at 12,000 rpm for 15 min for layer separation. The top transparent layer was carefully collected in a fresh tube, to which an equal volume of chilled isopropanol was added and incubated for 10 min at 4°C. RNA pellet was obtained by centrifugation for 15 min at 12,000 rpm, and was subsequently washed with freshly prepared 75% ethanol (molecular grade ethanol prepared in nuclease-free [NF] water). RNA pellet was eluted in 30–40 μ L of NF-water. Extracted RNA quality was assessed using a 1.2% agarose gel and quantified using a spectrophotometer (Nanodrop, Thermo Scientific, USA). A good quality RNA was then subjected to DNase treatment followed by reverse transcription for cDNA synthesis using a commercially available kit (ThermoFisher Scientific, DNase, and RevertAid cDNA synthesis kit). Gene expression analysis was performed using quantitative Real-time PCR (Quantitative PCR [qPCR]) employing iTaq Universal SYBR Green Supermix (Bio-Rad, California, United States) using different primers [Table 1]. qPCR was carried out on CFX96 Touch Real-Time PCR Detection System (Bio-Rad) conditions having (initial denaturation at 95°C, 2 min, followed by denaturation at 95°C, 5 s; annealing/extension at 60°C for 30 s) \times 40 cycles, final extension was done at 60°C for 5 min and melt curve conducted between 60°C and 95°C with 0.5°C/5 s increase. Data were interpreted using the $2^{-\Delta\Delta Ct}$ approach, with β -actin serving as a housekeeping gene for normalization.

2.13. Statistical Analysis

The data are depicted as the mean \pm standard error of the mean, calculated from triplicate measurements. Data analysis was performed using GraphPad Prism 8 software to ensure statistical accuracy and reliability. Statistical differences between groups were evaluated using one-way ANOVA, followed by Tukey's *post hoc* test for multiple comparisons. Statistical significance was presented as $P^* < 0.05$, $** < 0.01$, and $*** < 0.001$ versus the control group, as used in the results.

3. RESULTS

3.1. Phytochemical Analysis

Preliminary phytochemical analysis revealed the presence of a diverse range of phytochemical classes such as terpenoids, protein and amino acids, glycosides, alkaloids, saponins, carbohydrates, steroids, flavonoids, and phenols [Table 2].

3.2. Au-NPs Using Leaf Extract

HAuCl_4 acts as a gold precursor, and the extract of *L. speciosa* performs the dual function of stabilizing and reducing agent in the synthesis process. The color change was observed, which is the primary indication of bio-reduction of HAuCl_4 after adding the extract, as shown in Figure 1. The reaction mixture immediately changed color from pale yellow to ruby pink in 3 min, confirming the synthesis of Au-NPs.

3.3. UV-Visible Spectroscopy

The UV-visible spectra confirm the presence of Au-NP synthesis from leaf extract. The results show that tetrachloroaurate addition results in the appearance of a sharp peak at 546 nm; however, there is no apparent peak for the extract [Figure 2].

3.4. Zeta Potential/Zeta Sizer Study

The ± 30 mV zeta potential value of the dissolved suspension is needed for the stability of Au-NPs. The ± 20 mV potential is necessary for the steric and electrostatic combined effect. [43]. The zeta potential value -32.8 was recorded for leaf extract-synthesized Au-NPs [Figure 3]. Thus, the Au-NPs show values within permissible acceptable stability limits. Nanomaterials are in the size range of 1–100 nm in diameter. The average size of 75 nm was recorded [Figure 4]. The zeta size results also concur with the size permissible limits [44].

3.5. XRD

XRD patterns of the powdered sample indicated that the synthesized Au-NPs are crystalline. XRD spectrum results depict an intense peak at $2\theta = 38.1^\circ, 45.2^\circ, 64.7^\circ, 77.4^\circ, \text{ and } 82.1^\circ$, which correspond to the 111, 200, 220, 311, and 222 planes, indicating that the Au-NPs adopt face center cubic structure [Figure 5]. However, the crystal structure of pure metallic Au-NPs is observed.

3.6. FTIR

ATR-FTIR analysis of the synthesized Au-NPs shows various functional groups based on different frequency ranges, namely 1002 cm^{-1} representing the C-C and C-O stretching [45], 1318 cm^{-1} represents the C-N and aromatic amine [46], 1517 cm^{-1} represents the N-H bond [47], 1742 cm^{-1} indicates the presence of CHO or aldehyde group [48], and 3647 cm^{-1} indicates the presence of the OH alcoholic functional group [49] as depicted in Figure 6 and Table 3.

3.7. SEM

The analyzed FE-SEM images revealed that the generated particles mainly consist of spherical, poly-crystalline nature. Crystalline Au-NPs are examined using different magnifications, namely $\times 25,000$ and $\times 50,000$ for the particle size and morphological analysis. The resulting finding concluded that the synthesized gold particles have an average size within the 39.4–57.4 nm range [Figure 7].

3.8. TEM

The result obtained from the leaf extract of *L. speciosa* indicates the size and shape of the nanoparticles. Nanoparticles synthesized in the present study range from 1 nm to 100 nm, as shown in the HR-TEM images. TEM results support the conclusive finding of the SEM regarding shape and size. Selected area electron diffraction (SAED) pattern and XRD peak of spherical shape purified nanoparticles lie in their ability to confirm phase structure and crystallinity. SAED produces a diffraction pattern in the form of a concentric ring, and each

Table 1: List of primers used in expression analysis.

S. No.	Gene	Gene	Forward sequence (5'-3')	Reverse sequence (5'-3')
1	Beta-actin	β -ACTIN	ACTCCTATGTGGGTGACGAG	CACGGTTGGCCTTAGGGTT
2	CCAAT enhancer-binding protein alpha	C/EBP- α	CAGGGCAGGAGGAAGATACA	GGAAACCTGGCCTGTTGTAA
3	Fatty acid-binding protein	FABP-4/ap2	TCAGCGTAAATGGGGATTGGT	GTCGACTTCCATCCCCTTC
4	Peroxisome proliferator-activated receptor gamma	PPAR- γ	TCGCTGATGCACTGCCTAG	GGGTCAGCTCTTGTGAATGG

ring corresponds to the (111), (201), (220), (311), and (222) planes, matching the XRD result. The complementarity between the XRD and SAED ring patterns confirms the phase purity [Figure 8]. Results show similar trends as reported in previous studies [50].

Table 2: Qualitative phytochemical analysis of the *Lagerstroemia speciosa* fruit extract.

Compound types	Specific test	Positive indication	Results
Alkaloids	Wagner's reagent test	White/creamy ppt	++
Carbohydrates	Molish test	Red precipitate	+
Glycosides	Benedict's test	Precipitate	+
Saponins	Hemolytic assay	Foam	+
Terpenoids	Liebermann-Burchard's test	Pink-purple color	++
Steroids	Salkowski test	Red color	+
Phenols	Lead acetate test	Dark-green	+++
Protein and amino acids	Ninhydrin test	Purple color	++
Flavonoids	Alkaline reagent test	Crimson color	+

(+) indicated the presence/intensity of the phytochemical group in the tested sample.

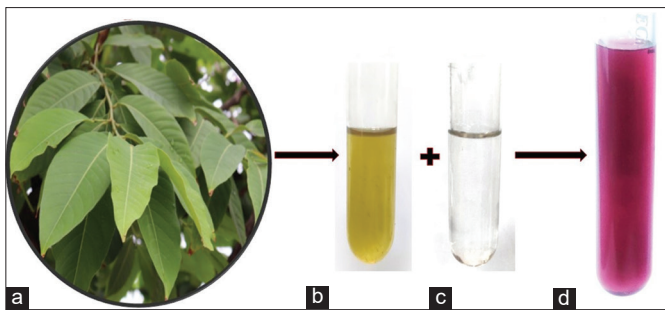


Figure 1: Fresh leaf of *Lagerstroemia speciosa* (a), aqueous leaf extract (b), aqueous gold nanoparticles (Au-NPs) solution (c), ruby pink colloidal solution of synthesized Au-NPs (d).

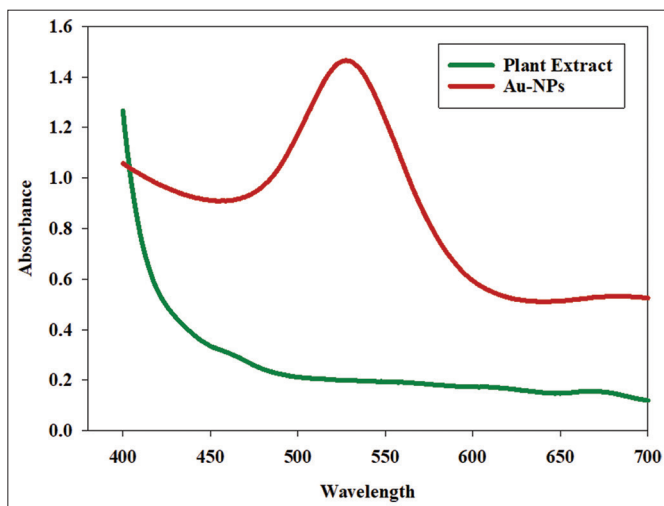


Figure 2: Comparative ultraviolet-visible absorption spectra of leaf extract and synthesized gold nanoparticles.

3.9. Effect of Different Extracts and their Au-NPs on Cell Viability

The findings demonstrate that increasing the concentration of aqueous, SFE, and biogenic GNPs to 200 $\mu\text{g/mL}$ does not show severe cytotoxicity, but in the case of methanol and n-hexane extract, it clearly shows cytotoxicity above 100 $\mu\text{g/mL}$. The percentage cell viability for aqueous (200 $\mu\text{g/mL}$), methanol (100 $\mu\text{g/mL}$), SFE (200 $\mu\text{g/mL}$), n-hexane (100 $\mu\text{g/mL}$), and AuNPs (200 $\mu\text{g/mL}$)

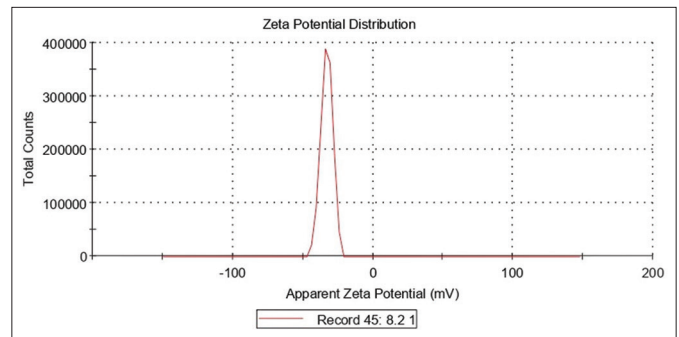


Figure 3: Zeta potential values of the synthesized *Lagerstroemia speciosa* gold nanoparticles.

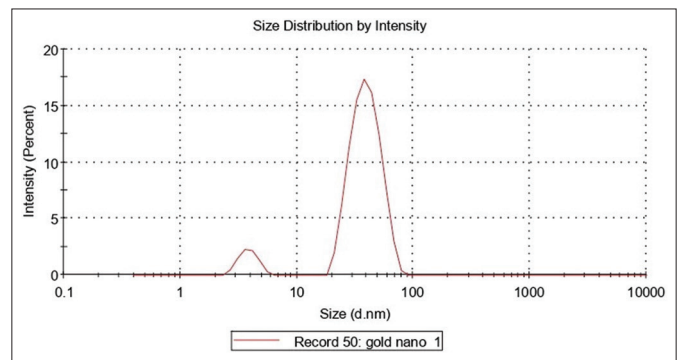


Figure 4: Zeta size distribution values of the synthesized gold nanoparticles.

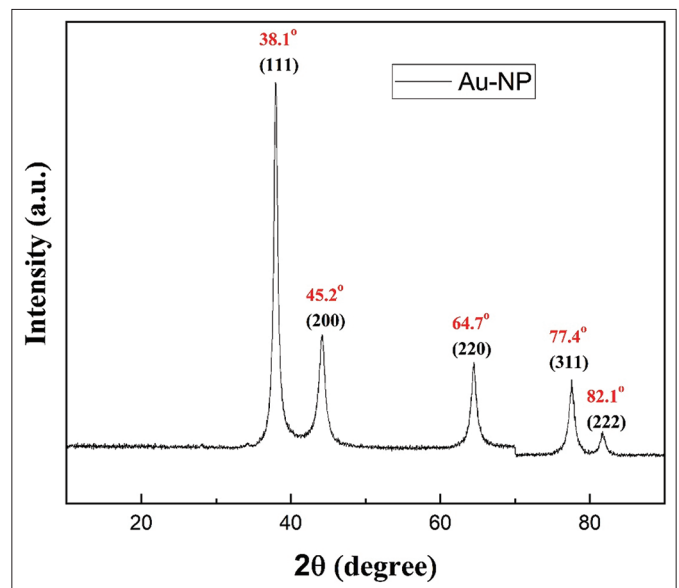


Figure 5: X-ray diffraction pattern of synthesized gold nanoparticles.

at optimal suitable dose is 79.50 ± 05.87 , 75.17 ± 09.58 , 75.31 ± 14.17 , 79.73 ± 01.76 , and 81.01 ± 04.49 , respectively [Figure 9]. The findings are consistent with the results of previous studies [51]. Treatment inhibits cell viability in a dose-dependent manner. The cytotoxic activity of *L. speciosa* leaf extracts prepared in different solvents was assessed through dose-response curves using linear regression analysis and showed acceptable linearity, with R^2 values of 0.967 (L-AQ), 0.8818 (L-MET), 0.9552 (L-SFE), 0.806 (L-HEX), and 0.9595 (L-AuNPs). The cytotoxic activity was evaluated through three independent experiments, and the IC_{50} values are reported as mean \pm standard error of the mean ($\mu\text{g/mL}$). The IC_{50} values obtained for the respective extracts were $366.243 \pm 27.271 \mu\text{g/mL}$, $227.797 \pm 23.249 \mu\text{g/mL}$, $309.772 \pm 29.969 \mu\text{g/mL}$, $240.191 \pm 13.758 \mu\text{g/mL}$, and $328.492 \pm 21.115 \mu\text{g/mL}$ [Table 4 and Figure 10].

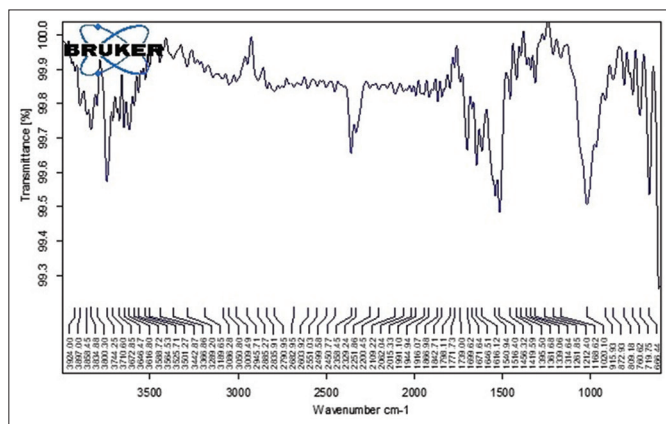


Figure 6: Attenuated total reflection-Fourier-transform infrared spectroscopy spectra of gold nanoparticles synthesized from leaf extract.

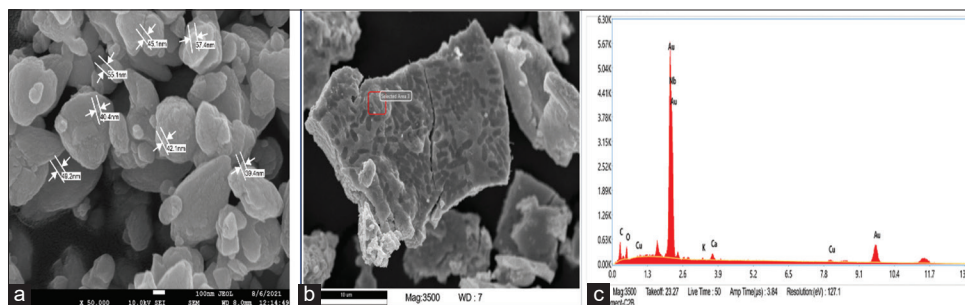


Figure 7: Field emission scanning electron microscopy image of gold nanoparticles at 50,000 magnification (a), energy dispersive X-ray scanning electron microscopy selected area (b), Energy-Dispersive X-ray microanalysis of gold nanoparticles (c).

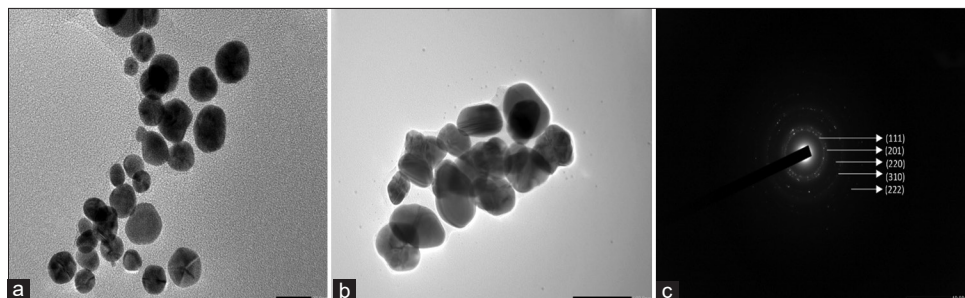


Figure 8: (a-c) High-resolution-transmission electron microscopy characterization of gold nanoparticles (AuNPs) on electron micrographs showed that LP-AuNPs are predominantly spherical in shape and crystalline in nature.

3.10. Effect of Extracts and Au-NPs Treatment on Lipid Accumulation Inhibition

Morphological alterations were observed in *L. speciosa* extracts and Au-NPs subjected to 3T3-L1 cells, transitioning from a spindle-like appearance before differentiation to a rounded shape post-differentiation. In addition, microscopic examination of ORO-stained lipid droplets within the cells indicated a dose-dependent reduction in lipid content in the case of extracts and Au-NPs-treated cells compared to the control group. Absorbance measurements indicated a concentration-dependent decrease in lipid accumulation in 3T3-L1 adipocytes. After treatment, the control or untreated cells exhibited the highest lipid droplet accumulation compared to the treated cells. Au-NPs-treated cells resulted in the highest reduction in lipid content (44.13%), followed by SFE (40.65%), aqueous (39.67%), methanol (27.02%), and n-hexane extract (15.41%) [Figures 11 and 12].

3.11. Effect of Au-NPs and Leaf Extracts on ROS Level

The process of adipogenesis, in which preadipocytes develop into mature adipocytes, is induced in the presence of dexamethasone, methyl isobutyl xanthine, and insulin [52]. Free fatty acids have been reported to generate ROS in various cell types, including adipocytes. The amount of ROS produced or reduced was quantified based on fluorescent intensity. The present investigation reveals that pretreatment with *L. speciosa* leaf aqueous, methanol, hexane, SFE, and AuNPs reduced the ROS production to 22.99%, 17.41%, 07.46%, 30.30%, and 43.35%, respectively, in 3T3-L1 cells at the maximum dose (200 $\mu\text{g/mL}$) compared with the control [Figure 13]. However, leaf methanol, hexane, SFE, and Au-NPs show significant change at the middle dose (100 $\mu\text{g/mL}$), also as compared to the control. The reduction in ROS was subsequently visualized using a confocal microscope, with cells subjected to different concentrations of 50, 100, and 200 $\mu\text{g/mL}$, while untreated cells served as controls. The images

Table 3: Fourier-transform infrared spectroscopy frequency range and functional groups present in the synthesized gold nanoparticles.

S. No.	Frequency range (cm ⁻¹)	Functional group
1.	665	Halogen group
2.	787	C-C, aromatic compounds
3.	1002	C-C, C-O stretching, either group
4.	1318	C-N stretch, aromatic amine
5.	1457	C=O stretching
6.	1517	N-H bond and amine groups
7.	1645	C=O stretching
8.	1697	C=O bond and aromatic ketones
9.	1742	CHO, aldehyde groups
10.	2360	P-, phosphine group
11.	3616	O-H group
12.	3647	OH, alcoholic groups
13.	3673	N-H, amide bond
14.	3744	OH, group of amides

Table 4: IC₅₀ values of different leaf extract and synthesized gold nanoparticles.

Test samples	IC ₅₀ values
L-AQ	366.243±27.271
L-MET	227.797±23.249
L-SFE	309.772±29.969
L-HEX	240.191±13.758
L-AuNPs	328.492±21.115

Results as Mean±SEM of triplicate.

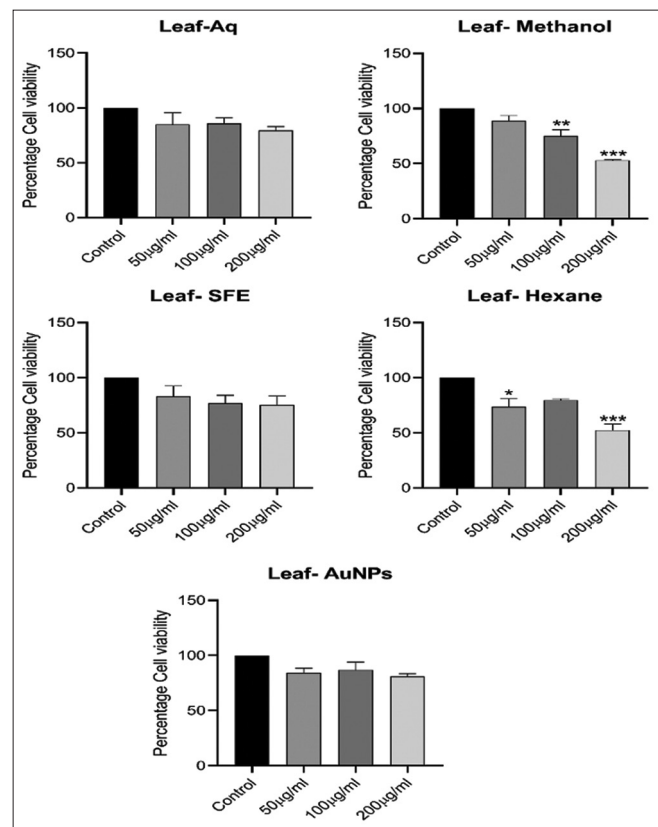
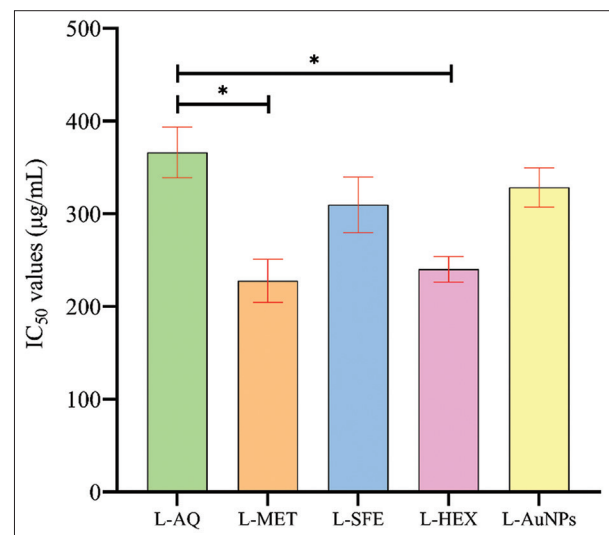
demonstrated a similar trend in ROS reduction, as shown in Figure 14. This decrease in ROS production highlights the therapeutic potential of *L. speciosa* as a promising treatment for ROS-related ailments.

3.12. Effect of Extracts and AuNPs on Triglyceride Accumulation

Treatment with leaf aqueous extract (100 and 200 µg/mL) resulted in a decrease in the triglyceride level by 59.29% and 56.95%, respectively. 100 and 200 µg/mL leaf methanol extract significantly lowers the triglyceride level by 62.75% and 57.56%, respectively, compared with the control. 100 µg/mL leaf SFE extract significantly reduced the triglyceride content by 57.87%. Further, leaf AuNPs (100 and 200 µg/mL) significantly lower the triglyceride level in 3T3-L1 adipocytes by 63.26% and 48.61%, respectively, compared with the control [Figure 15].

3.13. Effect on mRNA Expression Levels of Adipogenic Genes

Pre-treatment with leaf aqueous and AuNPs (100 and 200 µg/mL) significantly downregulated the mRNA expression levels of adipogenic genes (PPAR-γ, CEBP-α, and ap2/FABP4) compared with the control. However, methanol and SFE extracts show significant downregulation of these genes at higher doses (200 µg/mL). Further, the n-hexane

**Figure 9:** The effect of different doses of *Lagerstroemia speciosa* leaf extracts and gold nanoparticles on the cell viability of 3T3-L1 adipocytes. All values are expressed as mean ± standard error of the mean, n = 3.**Figure 10:** IC₅₀ values of different leaf extracts and synthesized gold nanoparticles.

leaf extract displayed no considerable effect on adipogenic markers [Figure 16].

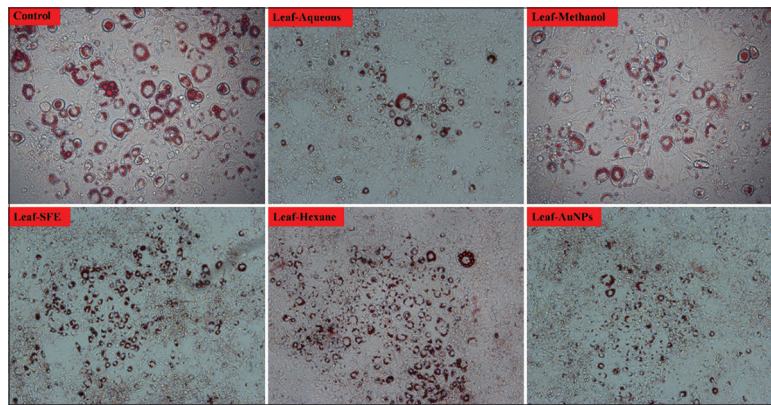


Figure 11: Effects of *Lagerstroemia speciosa* leaf extracts and gold nanoparticle treatment on the accumulation of lipids in 3T3-L1 cells. Oil-Red-O staining of the treated cells versus the controls.

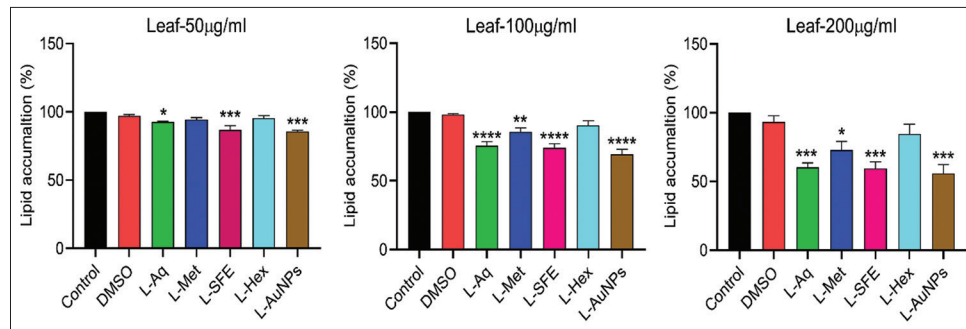


Figure 12: Different doses of *Lagerstroemia speciosa* leaf extracts and gold nanoparticles affect the cellular lipid accumulation in differentiated 3T3-L1 adipocytes. All values are expressed as mean \pm standard error of the mean, $n = 3$.

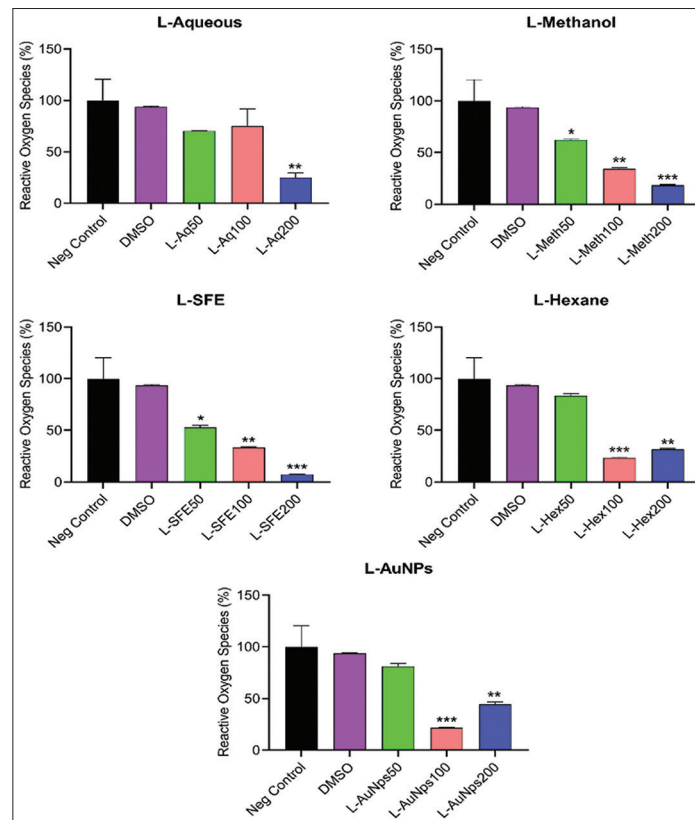


Figure 13: Effect of *Lagerstroemia speciosa* leaf extracts and their synthesized gold nanoparticles on markers reactive oxygen species level in 3T3-L1 adipocyte cells. All values are expressed as mean \pm standard error of the mean, $n = 3$.

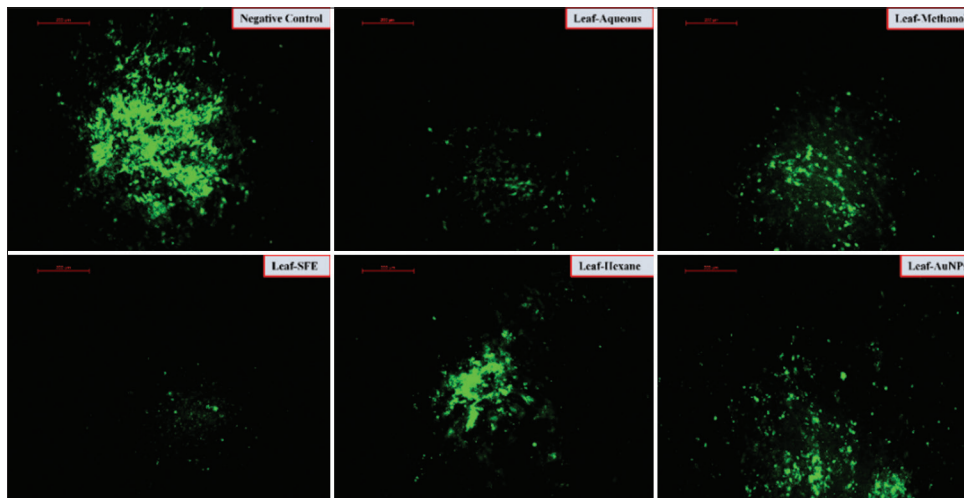


Figure 14: Effective inhibition of reactive oxygen species production by *Lagerstroemia speciosa* leaf extracts and gold nanoparticles in 3T3-L1 cells imaged by confocal microscope using the H₂DCFDA dye.

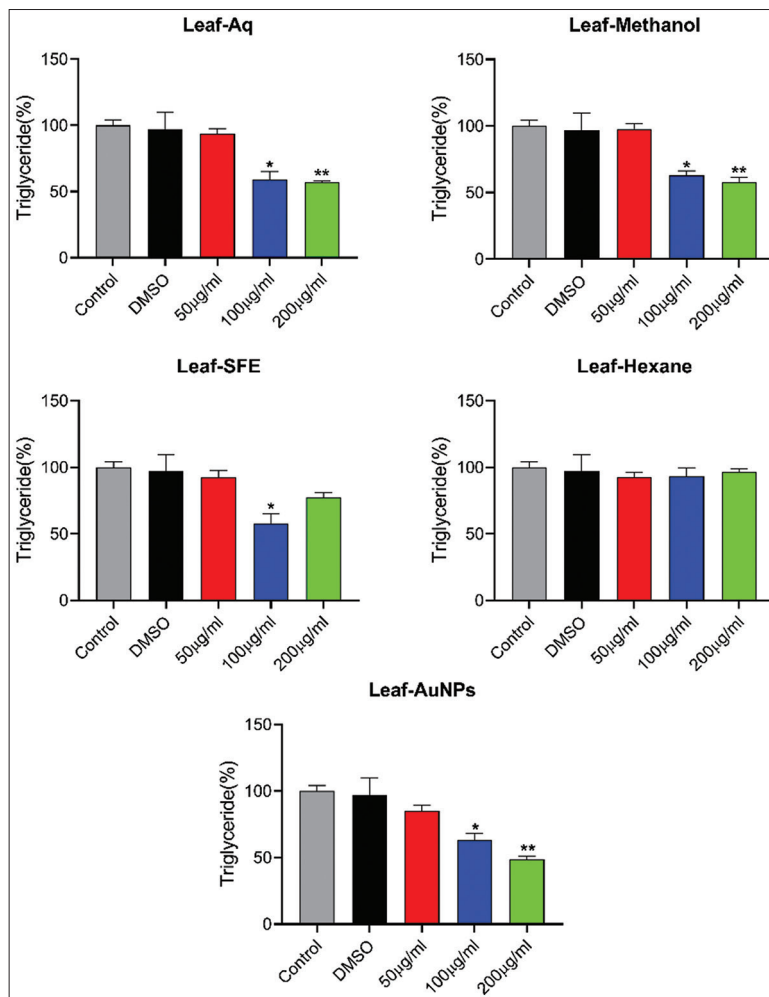


Figure 15: Effects of different leaf extracts of *Lagerstroemia speciosa* on triglyceride accumulation in 3T3-L1 adipocyte cells at different concentrations. All values are expressed as mean \pm standard error of the mean, $n = 3$.

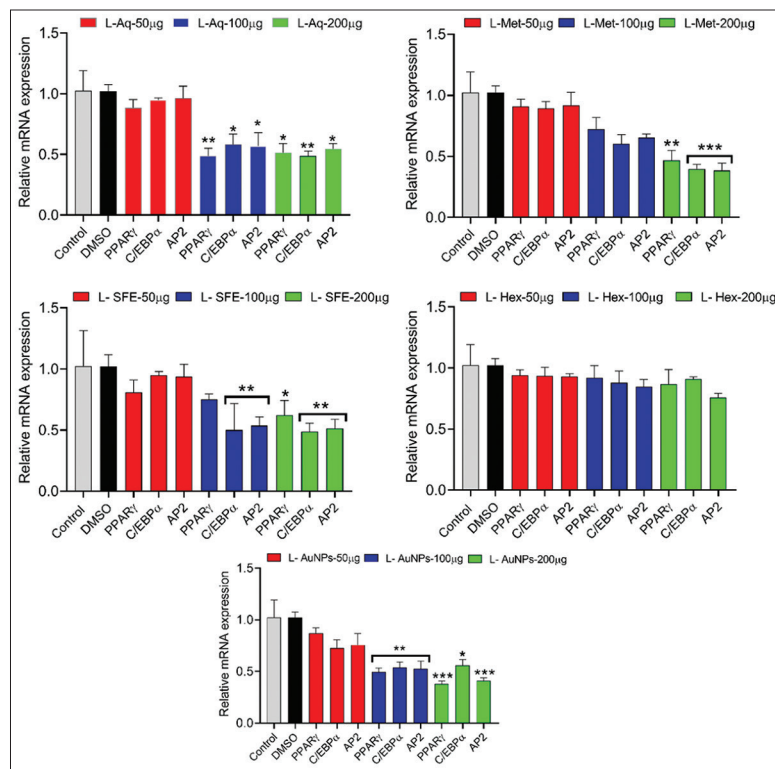


Figure 16: Effect of leaf extracts and gold nanoparticles of *Lagerstroemia speciosa* on adipogenesis markers in 3T3-L1 adipocyte cells. All values are expressed as mean \pm standard error of the mean, $n = 3$.

4. DISCUSSION

Obesity is one of the significant health issues adversely affecting nearly all physiological functions of the body, leading to co-morbidities such as diabetes mellitus, cardiovascular diseases, cancers, poor mental health, and many more [53-55]. Anti-obesity medications are pharmacological agents that modulate one of the three key metabolic mechanisms of body weight management, i.e., altering appetite, consuming calories, or metabolism. The possible adverse effects of these drugs (enhanced cardiovascular stroke, depression, suicidality, formation of kidney stones, and hyperoxaluria) outweigh their beneficial effects. The dismal history and depressing track record of anti-obesity medications serve as sufficient evidence for the need to look for alternative treatment options [56,57]. Natural products, particularly medicinal plants in the form of pure compounds or extracts, are widely available on the market as alternatives to conventional treatments and their associated challenges [58]. Phytochemicals can exhibit anti-adipogenic effects through diverse molecular mechanisms, by the inhibition of digestive enzymes (amylase and pancreatic lipase), regulation of appetite, and reduction in the accumulation of white adipose tissue (WAT) or promotion of WAT browning [59]. *L. speciosa* is a medicinal and horticultural plant containing bioactive phytochemicals widely reported to have hypoglycemic, anti-hyperlipidemic, antioxidant, anti-diabetic, and anti-obesity activity [60]. In the present study, the leaf extract of *L. speciosa* in different solvents such as water, methanol, SFE, and hexane and leaf-mediated Au-NPs were used to assess the impact of these extracts on lipolysis, lipolysis, and adipogenesis in 3T3-L1. Adipogenesis plays a critical role in the development of obesity [1]. In obesity, adipose tissue grows by hypertrophy (cell size increase) and hyperplasia (cell number increase) to store more lipids [61]. Increasing lipid deposition in adipocytes is a crucial aspect of adipogenesis. The present investigation found that leaf aqueous, SFE extract, and Au-NPs treatments showed

an inhibitory effect on adipogenesis and lipid accumulation in 3T3-L1 cells at their maximum doses. While n-hexane showed no significant change after treatment, as shown in Oil-Red O staining, it reduced the lipid droplet size and suppressed oil droplet accumulation on differentiated cells. Furthermore, research findings revealed the reduced lipid accumulation in the triglyceride assay after treatment with leaf aqueous, SFE extract, and AuNPs. These extracts show inhibitory effects on lipid accumulation and triglyceride content. Down-regulation of CEBP- α , PPAR- γ , Jak-2, STAT3, and ap2 expression in 3T3-L1 cells in the recently reported results follows similar trends in the obesity control approach [36]. *Panax ginseng* leaf shows similar trends of PPAR- γ /CEBP- α and ap2 signaling suppression in the case of 3T3-L1 mature adipocytes [62]. *In silico* targeting of PPAR- γ /CEBP- α in the case of *Terminalia ferdinandiana* follows a similar trend of obesity regulation [63]. Ethanolic leaf extract of *Pinus koraiensis* down-regulates the expression of the PPAR- γ /CEBP- α transcriptional gene by activating the AMPK pathway, which results in controlling obesity. The present study also revealed the same results [64]. In addition, another study on the DLBS3733 fraction from *L. speciosa* lowers fat droplets by inhibiting adipogenesis and lipogenesis [65]. Adipocyte maturation and fat storage occur during the onset and progression of obesity. Adipocytes, during differentiation, produced an increased amount of ROS, which could possibly be due to the activation of NADPH oxidase and an increase in the concentration of fatty acids [66]. Findings from the study demonstrate that treatment with leaf extracts and AuNPs of *L. speciosa* at different doses decreased ROS production in 3T3-L1 cells. Adipocyte differentiation during adipogenesis is mainly induced by C/EBP- α and PPAR- γ [67]. PPAR- γ and C/EBP are key transcriptional signaling molecules of adipogenesis, resulting in the expression of genes associated with lipolysis, lipogenesis, adipocyte protein 2, and insulin sensitivity, including glucose transporter 4 [68]. The reduction of

adipose tissue level has recently been considered an effective approach in obesity management, and based on the present findings, leaf aqueous, methanol, SFE extracts, and leaf Au-NPs treatment at different dosages inhibited adipogenesis, as confirmed by the reduction of adipogenic marker genes, which include PPAR- γ , C/EBP- α , and aP2. The present study lacks a complete upstream pathway, such as AMPK, MAPK, and NF- κ B analysis, which elucidates the link between nanoparticle action and adipogenic signaling cascade. However, further *in vivo* studies incorporating Western blot analysis are required to validate conclusive findings.

The pharmacokinetics, biodistribution, long-term safety, and immunogenicity of Au-NPs are size- and surface-dependent. Smaller size of Au-NPs typically exhibits extended circulatory half-lives compared to larger particles. Their surface modification significantly influences opsonization and circulation time. Across multiple studies, the liver and spleen are the principal sinks for systemically administered Au-NPs due to Kupffer cell uptake. Au-NPs can persist in organs long-term, potentially causing mild inflammation or fibrosis, warranting chronic toxicity evaluation. *In vitro* exposure of 3T3-L1 cells with Au-NPs internalizes primarily through endocytosis. The uptake potential determines the intracellular concentration, which later on affects the downstream biological processes such as lipid accumulation, ROS generation, triglyceride accumulation, and modulation of gene expression of adipogenic markers, namely C/EBP- α , PPAR- γ , and aP2. Previously reported results with synthesized Au-NPs with fresh *Panax ginseng* leaf extract suppress adipogenesis by downregulating PPAR- γ and C/EBP- α signaling in 3T3-L1 mature adipocytes [62]. Similar kinds of reports of *Cinnamomum verum* biosynthesized Au-NPs in obesity control approaches are described in recent findings after detailed characterization through FE-SEM, TEM, FTIR, and XRD techniques [69]. The decreased lipid accumulations and triglyceride storage in 3T3-L1 cells in the present study might be due to the downregulation of PPAR/CEBP signaling and downstream genes by leaf extracts and Au-NPs of *L. speciosa*. Based on cytotoxicity analysis, the developed nanoparticles demonstrate a favorable biosafety profile and potential human applicability, showing minimal toxicity and good biocompatibility, thereby supporting their promise for clinical translation.

5. CONCLUSION

Recent investigations have intensely focused on obesity and its related metabolic disorders. To explore potential therapeutic tools for addressing obesity and obesity-triggered problems, the study investigates the comparative effect of *L. speciosa* leaf extract and its synthesized nanoparticles. The results showed a significant reduction in the ROS generation level. Treatment with different leaf extracts and Au-NPs also decreases the lipid accumulation and triglyceride content within the cells. Adipogenic factors PPAR- γ and C/EBP- α are downregulated after treatment with plant extract and Au-NPs. Aqueous, SFE extract, and Au-NPs show maximum effects, methanol extract shows a moderate effect, and n-hexane shows a negligible impact on gene expression regulation. As the present study is *in vitro*, further *in vivo* studies are required to validate these results, confirm their safety, and support developing and applying novel herbal nanoparticles for human health benefits.

6. ACKNOWLEDGMENT

The authors gratefully acknowledge MDU Rohtak, for providing the University Research Scholarship (URS), which supported Tarsem Nain in carrying out this work, and also thank the National Agri-Food

Biotechnology Institute (NABI), Mohali, for their technical support and access to laboratory facilities.

7. AUTHORS' CONTRIBUTIONS

All authors made substantial contributions to conception and design, acquisition of data, or analysis and interpretation of data; took part in drafting the article or revising it critically for important intellectual content; agreed to submit to the current journal; gave final approval of the version to be published; and agreed to be accountable for all aspects of the work. All the authors are eligible to be authors as per the International Committee of Medical Journal Editors (ICMJE) requirements/guidelines.

8. CONFLICTS OF INTEREST

The authors report no financial or any other conflicts of interest in this work.

9. ETHICAL APPROVALS

This study does not involve experiments on animals or human subjects.

10. DATA AVAILABILITY

All data generated and analysed are included within this research article.

11. PUBLISHER'S NOTE

All claims expressed in this article are solely those of the authors and do not necessarily represent those of the publisher, the editors and the reviewers. This journal remains neutral with regard to jurisdictional claims in published institutional affiliation.

12. USE OF ARTIFICIAL INTELLIGENCE (AI)-ASSISTED TECHNOLOGY

The authors declare that they have not used artificial intelligence (AI)-tools for writing and editing of the manuscript, and no images were manipulated using AI.

REFERENCES

- Xu L, Yang C, Pang K, Zhang Y, He Y, Liu S, *et al.* Adipocyte Septin-7 attenuates obesogenic adipogenesis and promotes lipolysis to prevent obesity. *Mol Metab.* 2025;95:102114.
- Blüher M. Obesity: Global epidemiology and pathogenesis. *Nat Rev Endocrinol.* 2019;15(5):288-98.
- Kobi JB, Matias AM, Gasparini PV, Torezani-Sales S, Madureira AR, da Silva DS, *et al.* High-fat, high-sucrose, and combined high-fat/high-sucrose diets effects in oxidative stress and inflammation in male rats under presence or absence of obesity. *Physiol Rep.* 2023;11(7):e15635.
- Mohamed MM, Kamel EA, Ahmed KA, Rashed LA, Ismail SH. The potential efficacy of *Artemisia annua* L. extract nanoparticles in mitigating obesity-related-metabolic complications in hypercaloric diet-fed rats. *Egypt J Basic Appl Sci.* 2024;11(1):183-212.
- Geng X, Tian W, Zhuang M, Shang H, Gong Z, Li J. Green radish polysaccharides ameliorate hyperlipidemia in high-fat-diet-induced mice via short-chain fatty acids production and gut microbiota regulation. *Foods.* 2024;13(24):4113.
- Kazemi N, Ramazani E, Tayarani-Najaran Z. *In vitro* effects of phytochemicals on adipogenesis with a focus on molecular mechanisms: A systematic review. *Iran J Basic Med Sci.*

- 2025;28(4):409-25.
7. Chandrasekaran A, Jeon Y, Kim SY, Seo DH, Yuk HJ, Son E, *et al.* Therapeutic potential of suaeda *Japonica makino* leaf extract against obesity in 3T3-L1 preadipocytes and HFD-induced C57BL/6 J mice. *Appl Biochem Biotechnol.* 2025;197:2555-78.
 8. Christoffersen BØ, Sanchez-Delgado G, John LM, Ryan DH, Raun K, Ravussin E. Beyond appetite regulation: Targeting energy expenditure, fat oxidation, and lean mass preservation for sustainable weight loss. *Obesity (Silver Spring).* 2022;30(4):841-57.
 9. Tak YJ, Lee SY. Anti-obesity drugs: Long-term efficacy and safety: An updated review. *World J Mens Health* 2020;39(2):208-21.
 10. Nagre K, Singh N, Ghoshal C, Tandon G, Iquebal MA, Nain T, *et al.* Probing the potential of bioactive compounds of millets as an inhibitor for lifestyle diseases: Molecular docking and simulation-based approach. *Front Nutr.* 2023;10:1228172.
 11. Yue Z, Xu Y, Cai M, Fan X, Pan H, Zhang D, *et al.* Floral elegance meets medicinal marvels: Traditional uses, phytochemistry, and pharmacology of the genus *Lagerstroemia* L. *Plants (Basel).* 2024;13(21):3016.
 12. Al-Snafi AE. Medicinal value of *Lagerstroemia speciosa*: An updated review. *Int J Curr Pharm Res.* 2019;11(5):18-26.
 13. Yin H, Yang X, Liu S, Zeng J, Chen S, Zhang S, *et al.* Total flavonoids from *Lagerstroemia speciosa* (L.) Pers inhibits TNF- α -induced insulin resistance and inflammatory response in 3T3-L1 adipocytes via MAPK and NF- κ B signaling pathways. *Food Sci Technol.* 2022;42:e45222.
 14. Unno T, Sugimoto A, Kakuda T. Xanthine oxidase inhibitors from the leaves of *Lagerstroemia speciosa* (L.) Pers. *J Ethnopharmacol.* 2004;93(2-3):391-5.
 15. Gupta A, Agrawal VK, Rao CV. Exploration of analgesic and antiinflammatory potential of *Lagerstroemia speciosa*. *J Appl Pharm Sci.* 2017;7(2):156-61.
 16. Chowdhury MA, Islam MR, Muktadir MA. Thrombolytic activity of *Lagerstroemia speciosa* Leaves. *Discov Phytomed.* 2017;4(4):41-5.
 17. Sahu BD, Kuncha M, Rachamalla SS, Sistla R. *Lagerstroemia speciosa* L. attenuates apoptosis in isoproterenol-induced cardiotoxic mice by inhibiting oxidative stress: Possible role of Nrf2/HO-1. *Cardiovasc Toxicol.* 2015;15:10-22.
 18. Goyal S, Sharma M, Sharma R. Bioactive compound from *Lagerstroemia speciosa*: Activating apoptotic machinery in pancreatic cancer cells. *3 Biotech.* 2022;12(4):96.
 19. Tandrasasmita OM, Berlian G, Tjandrawinata RR. Molecular mechanism of DLBS3733, a bioactive fraction of *Lagerstroemia speciosa* (L.) Pers., on ameliorating hepatic lipid accumulation in HepG2 cells. *Biomed Pharmacother.* 2021;141:111937.
 20. Chaudhary G, Mahajan UB, Goyal SN, Ojha S, Patil CR, Subramanya SB. Protective effect of *Lagerstroemia speciosa* against dextran sulfate sodium induced ulcerative colitis in C57BL/6 mice. *Am J Transl Res.* 2017;9(4):1792-800.
 21. Amith T, Sujatha P. Anticalciuria effect of methanolic root extract of *Lagerstroemia speciosa* (L.) pers (*Lythraceae*) against high protein diet ingested in albino rats. *J Adv Sci Res.* 2023;14(10):30-5.
 22. Pareek A, Suthar M, Rathore GS, Bansal V, Kumawat T. *In vitro* antioxidant studies of *Lagerstroemia speciosa* leaves. *Pharmacogn J.* 2010;2(10):357-60.
 23. Ganesan G, Sujatha P. Anti-obesity effects of *Lagerstroemia speciosa* ethanolic green and red leaf extracts against caprylic acid and a high fat diet in the albino rat. *Res J Agric Sci.* 2024;15(4):957-62.
 24. Hestiantoro A, Wiryawan P, Tjandrawinata RR, Wiweko B, Ritonga MA, Ferrina AI, *et al.* The efficacy and safety of DLBS3233, a combined bioactive fraction of *Cinnamomum burmanii* and *Lagerstroemia speciosa* plants on the endocrine-metabolic profile of women with polycystic ovary syndrome: A randomized clinical trial. *Int J Fertil Steril.* 2024;18(1):35-47.
 25. Shashiraj KN, Hugar A, Kumar RS, Rudrappa M, Bhat MP, Almansour AI, *et al.* Exploring the antimicrobial, anticancer, and apoptosis inducing ability of biofabricated silver nanoparticles using *Lagerstroemia speciosa* flower buds against the Human Osteosarcoma (MG-63) cell line via flow cytometry. *Bioengineering (Basel).* 2023;10(7):821.
 26. Singla R, Soni S, Kulurkar PM, Kumari A, Mahesh S, Patial V, *et al.* *In situ* functionalized nanobiocomposites dressings of bamboo cellulose nanocrystals and silver nanoparticles for accelerated wound healing. *Carbohydr Polym.* 2017;155:152-62.
 27. Pathan A, Nayak T, Alshahrani S, Tripathi R, Tripathi P. Current and emerging frontiers in biologically synthesized gold nanoparticles: An in-depth review. *Chem Pap.* 2025;79:3421-42.
 28. Sekhon-Loodu S, Rupasinghe HV. Evaluation of antioxidant, antidiabetic and antiobesity potential of selected traditional medicinal plants. *Front Nutr.* 2019;6:53.
 29. Kaushik S, Kaushik S, Dar L, Yadav JP. Eugenol isolated from supercritical fluid extract of *Ocimum sanctum*: A potent inhibitor of DENV-2. *AMB Express.* 2023;13(1):105.
 30. Namdev N. Forensic screening of medicinal plants for qualitative phytochemical analysis using various solvent extracts. *J Emerg Innov.* 2024;1(1):54-8.
 31. Wehbe N, Mesmar JE, El Kurdi R, Al-Sawalmih A, Badran A, Patra D, *et al.* *Halodule uninervis* extract facilitates the green synthesis of gold nanoparticles with anticancer activity. *Sci Rep.* 2025;15(1):4286.
 32. Hajighasemi N. Investigating the Stability of Different Sizes of Gold Nanoparticles in Physiological Environments and different Gold Nanoclusters in Water. Canada: The University of Western Ontario; 2024. p. 1-24.
 33. Singh P, Kim YJ, Wang C, Mathiyalagan R, Yang DC. The development of a green approach for the biosynthesis of silver and gold nanoparticles by using *Panax ginseng* root extract, and their biological applications. *Artif Cells Nanomed Biotechnol.* 2016;44(4):1150-7.
 34. Shah S, Shah SA, Faisal S, Khan A, Ullah R, Ali N, *et al.* Engineering novel gold nanoparticles using *Sageretia thea* leaf extract and evaluation of their biological activities. *J Nanostruct Chem.* 2022;12(1):129-40.
 35. Ahn S, Singh P, Jang M, Kim YJ, Castro-Aceituno V, Simu SY, *et al.* Gold nanoflowers synthesized using *Acanthopanax* cortex extract inhibit inflammatory mediators in LPS-induced RAW264. 7 macrophages via NF- κ B and AP-1 pathways. *Colloids Surf B Biointerfaces.* 2018;162:398-404.
 36. Yi MH, Simu SY, Ahn S, Aceituno VC, Wang C, Mathiyalagan R, *et al.* Anti-obesity effect of gold nanoparticles from *Dendropanax moribifera* Léveillé by suppression of triglyceride synthesis and downregulation of PPAR γ and CEBP α signaling pathways in 3T3-L1 mature adipocytes and HepG2 cells. *Curr Nanosci.* 2020;16(2):196-203.
 37. Rohmawaty E, Wiraswati HL, Zahra TA, Amalina SN, Ramadhanti J, Rosdianto AM, *et al.* Antioxidant and anti-inflammatory potential of *Cymbopogon nardus* ethanol extract on 3T3-L1 cells. *J Inflamm Res.* 2025;18:2125-36.
 38. Yu SY, Choi Y, Kwon YI, Lee OH, Kim YC. Mechanism of formononetin-induced stimulation of adipocyte fatty acid oxidation and preadipocyte differentiation. *J Food Nutr Res.* 2021;9(3):163-9.
 39. Kim D, Lee C, Kim M, Park JH. Gold kiwi-derived nanovesicles mitigate ultraviolet-induced photoaging and enhance osteogenic differentiation in bone marrow mesenchymal stem cells. *Antioxidants (Basel).* 2024;13(12):1474.
 40. Mohanty S, Pattnaik A. Evaluation of anti-obesity potential of isolated bioactive fractions from *Justicia Adhatoda* leaves: An *in vitro*, *in vivo*, and 3T3-L1 cell line approach using high-performance thin layer chromatography coupled with mass spectrometry for compound identification. *Chem Biodivers.* 2025;22(5):e202401532.
 41. Bustin SA, Benes V, Garson JA, Hellemans J, Huggett J, Kubista M,

- et al.* The MIQE Guidelines: Minimum Information for Publication of Quantitative Real-Time PCR Experiments. United Kingdom: Oxford University Press; 2009.
42. Nandi Jui B, Sarsenbayeva A, Jernow H, Hetty S, Pereira MJ. Evaluation of RNA isolation methods in human adipose tissue. *Lab Med.* 2022;53(5):e129-33.
 43. Jiao Y, Wang X, Chen JH. Biofabrication of AuNPs using *Coriandrum sativum* leaf extract and their antioxidant, analgesic activity. *Sci Total Environ.* 2021;767:144914.
 44. Dolai J, Mandal K, Jana NR. Nanoparticle size effects in biomedical applications. *ACS Appl Nano Mater.* 2021;4(7):6471-96.
 45. Li J, Zhang Y, Gao H, Wang D, Xue J, Chen X, *et al.* Characteristics study on the cofluidized thermal conversion of vacuum residue and rice husk pyrolysis oil. *Fuel.* 2024;365:131221.
 46. Alam MS, Lee DU. Molecular structure, spectral (FT-IR, FT-Raman, UV-Vis, and fluorescent) properties and quantum chemical analyses of azomethine derivative of 4-aminoantipyrine. *J Mol Struct.* 2021;1227:129512.
 47. Abdelhadi AB, Rodríguez-Sánchez S, Ouarsal R, Saadi M, El Ammari L, Morley N, *et al.* Synthesis, characterization, and magnetic and antibacterial properties of a novel iron (iii) complex (CH₃)₂NH₂[Fe(phen)Cl₄]. *Mater Adv.* 2024;5(7):3058-66.
 48. Tsague FL, Chimeni DY, Assonfack HL, Abo MT, Cheumani AM, Ndinteh DT, *et al.* Study of oxidation of cellulose by Fenton-type reactions using alkali metal salts as swelling agents. *Cellulose.* 2024;31(11):6643-61.
 49. Abbas HS, Ismaeil TA, Ahmed EA, Abou Baker DH. Iron oxide nanoparticles of *Cystoseira* sp. Sugar alcohol treat MRSA and thyroid gland cancer. *J King Saud Univ Sci.* 2024;36(8):103338.
 50. Jurkiewicz K, Pawlyta M, Burian A. Structure of carbon materials explored by local transmission electron microscopy and global powder diffraction probes. *C-J Carbon Res.* 2018;4(4):68.
 51. Akter R, Ling L, Rupa EJ, KyuPark J, Mathiyalagan R, Nahar J, *et al.* Binary effects of gynostemma gold nanoparticles on obesity and inflammation via downregulation of PPAR γ /CEBP α and TNF- α gene expression. *Molecules.* 2022;27(9):2795.
 52. Lee E, Nam JO. Anti-obesity and anti-diabetic effects of *Ostericum koreanum* (Ganghwal) extract. *Int J Mol Sci.* 2024;25(9):4908.
 53. Neill S, Driscoll L. Metabolic syndrome: A closer look at the growing epidemic and its associated pathologies. *Obes Rev.* 2015;16(1):1-12.
 54. Schetz M, De Jong A, Deane AM, Druml W, Hemelaar P, Pelosi P, *et al.* Obesity in the critically ill: A narrative review. *Intensive Care Med.* 2019;45(6):757-69.
 55. Polyzos SA, Kountouras J, Mantzoros CS. Obesity and nonalcoholic fatty liver disease: From pathophysiology to therapeutics. *Metabolism.* 2019;92:82-97.
 56. Daneschvar HL, Aronson MD, Smetana GW. FDA-approved anti-obesity drugs in the United States. *Am J Med.* 2016;129(8):879.e1-6.
 57. Velazquez A, Apovian CM. Updates on obesity pharmacotherapy. *Ann N Y Acad Sci.* 2018;1411(1):106-19.
 58. Najmi A, Javed SA, Al Bratty M, Alhazmi HA. Modern approaches in the discovery and development of plant-based natural products and their analogues as potential therapeutic agents. *Molecules.* 2022;27(2):349.
 59. Fu C, Jiang Y, Guo J, Su Z. Natural products with anti-obesity effects and different mechanisms of action. *J Agric Food Chem.* 2016;64(51):9571-85.
 60. Tripathi SK, Behera S, Panda M, Zengin G, Biswal BK. A comprehensive review on pharmacology and toxicology of bioactive compounds of *Lagerstroemia speciosa* (L.) Pers. *Curr Tradit Med.* 2021;7(4):504-13.
 61. Cheng Y, Zhang K, Liu J, Liu G. Is orbital adipose tissue obesity-privileged? The relationship between small adipocyte size and metabolically healthy state from the view of orbital fat. *J Endocrinol Invest.* 2025;48:1-14.
 62. Simu SY, Ahn S, Castro-Aceituno V, Singh P, Mathiyalagan R, Jiménez-Pérez ZE, *et al.* Gold nanoparticles synthesized with fresh *Panax ginseng* leaf extract suppress adipogenesis by downregulating PPAR γ /CEBP α signaling in 3T3-L1 mature adipocytes. *J Nanosci Nanotechnol.* 2019;19(2):701-8.
 63. Morshed MN, Awais M, Akter R, Park J, Ling L, Kong BM, *et al.* Exploring the therapeutic potential of *Terminalia ferdinandiana* (Kakadu Plum) in targeting obesity-induced Type 2 diabetes and chronic inflammation: An *in silico* and experimental study. *S Afr J Bot.* 2024;171:32-44.
 64. Lee MS, Cho SM, Lee MH, Lee EO, Kim SH, Lee HJ. Ethanol extract of *Pinus koraiensis* leaves containing lambertianic acid exerts anti-obesity and hypolipidemic effects by activating adenosine monophosphate-activated protein kinase (AMPK). *BMC Complement Altern Med.* 2016;16:51.
 65. Karsono AH, Tandrasasmita OM, Tjandrawinata RR. Bioactive fraction from *Lagerstroemia speciosa* leaves (DLBS3733) reduces fat droplet by inhibiting adipogenesis and lipogenesis. *J Exp Pharmacol.* 2019;11:39-51.
 66. Lee W, Song G, Bae H. Suppressive effect of fraxetin on adipogenesis and reactive oxygen species production in 3T3-L1 cells by regulating MAPK signaling pathways. *Antioxidants (Basel).* 2022;11(10):1893.
 67. Ree J, Kim JI, Lee CW, Lee J, Kim HJ, Kim SC, *et al.* Quinizarin suppresses the differentiation of adipocytes and lipogenesis *in vitro* and *in vivo* via downregulation of C/EBP-beta/SREBP pathway. *Life Sci.* 2021;287:120131.
 68. Mota de Sá P, Richard AJ, Hang H, Stephens JM. Transcriptional regulation of adipogenesis. *Compr Physiol.* 2017;7(2):635-74.
 69. Sharma VK, Gupta SC, Singh BN, Rao CV, Barik SK. *Cinnamomum verum* derived bioactives-functionalized gold nanoparticles for prevention of obesity through gut microbiota reshaping. *Mater Today Bio.* 2022;13:100204.

How to cite this article:

Nain T, Bishnoi M, Kaur N, Tiwari SK, Yadav JP. The comparative anti-obesity potential of *Lagerstroemia speciosa* (L.) leaf extracts and their synthesized gold nanoparticles by downregulation of PPAR- γ , C/EBP- α , and FABP4/aP2 gene expression. *J Appl Biol Biotech* 2026;14(1):143-155. DOI: 10.7324/JABB.2025.258124